



Acta Materialia 59 (2011) 4895-4906



www.elsevier.com/locate/actamat

In situ lorentz TEM magnetization study of a Ni–Mn–Ga ferromagnetic shape memory alloy

A. Budruk a, C. Phatak b, A.K. Petford-Long b, M. De Graef a,*

a Department of Materials Science and Engineering, Carnegie Mellon University, Pittsburgh, PA 15213, USA
b Argonne National Laboratory, 9700 S Cass Avenue, Argonne, IL 60439, USA

Received 12 January 2011; received in revised form 12 April 2011; accepted 14 April 2011 Available online 14 May 2011

Abstract

The magnetic domain structure of a $Ni_{49.9}Mn_{28.3}Ga_{21.8}$ ferromagnetic shape memory alloy has been investigated by in situ Lorentz TEM. Field-induced changes in the magnetic domain wall structure were recorded over a field range of [-500, +300] Oe. Inside a martensite twin variant, the observed domain structure was either an alternating 180° wall pattern or a maze-like pattern, depending on the relative orientation of the magnetic easy axis and the in-plane applied field. In twin variants with an in-plane easy axis, significant domain wall movement was observed at moderate applied fields, in agreement with an existing magneto-mechanical model. 180° domain walls were found to be pinned by anti-phase boundaries (APBs). The maze-like domain structure was stable under applied fields below about ± 100 Oe; at higher fields, the walls became aligned with the applied field. Domain walls also remained strongly pinned at twin boundaries up to applied fields of around 400 Oe. Interestingly, depinning of walls from twin boundaries occurs at field values that are significantly lower than those required to induce motion of the structural twins.

© 2011 Acta Materialia Inc. Published by Elsevier Ltd. All rights reserved.

Keywords: Lorentz microscopy; Heusler phases; Martensitic phase transformation; Magnetic domain; Twinning

1. Introduction

The phenomenon of giant magnetic field-induced strain (MFIS) in magnetic shape memory alloys (MSMAs) has attracted significant attention recently, because such materials can be used as actuators and sensors. Maximum recoverable strains of up to 9.5% have been reported in Ni–Mn–Ga alloys [1]. The underlying mechanism behind the magnetic field-induced strain in MSMAs can be described briefly as follows. The martensitic phase transformation responsible for the shape memory effect is inherently lattice distortive. Hence, the martensitic phase evolves

with a microstructure that minimizes the strain energy associated with the lattice distortion [2]. One way to minimize this strain energy is a mechanism known as selfaccommodation. During self-accommodation, different martensite variants are twinned with respect to each other so as to minimize the overall strain energy [3]. As the martensite is ferromagnetic, the magnetic easy axes of adjacent twin variants are at specific angles with respect to each other (typically close to 90°). The magnetic easy axis happens to coincide with the lattice direction associated with maximum contraction during the martensitic transformation. Under the application of a magnetic field, the variants with easy axes favorable to the magnetic field grow at the expense of unfavorably oriented variants [4]. The applied magnetic field is believed to exert a pressure on the twin boundaries due to the difference in Zeeman energy across the twin boundary [5]. If the twinning stresses are sufficiently low, this pressure causes twin boundary motion, which results in a significant amount of shape strain,

^{*} Corresponding author. Address: Department of Materials Science and Engineering, Carnegie Mellon University, 5000 Forbes Avenue, Pittsburgh, PA 15213-3890, USA.

E-mail addresses: abudruk@andrew.cmu.edu (A. Budruk), cd@anl. gov (C. Phatak), petford.long@anl.gov (A.K. Petford-Long), degraef@cmu.edu (M. De Graef).

which, in turn, manifests itself as a magnetic field-induced strain [6]. This reorientation of martensite variants is possible only when the martensite has a high magnetocrystalline anisotropy energy and a low twinning stress [5]. It is clear that the phenomenon of MFIS involves a strong interaction between magnetic domains and twin variants. Along with the martensitic transformation mentioned above, the Ni-Mn-Ga type alloys also undergo an atomic ordering transformation which results in the formation of ordered domains separated by anti-phase boundaries (APBs) [7]. The magnetic domain structure associated with the twin variants in Ni-Mn-Ga alloys has been studied mostly with the specimen in the demagnetized state, i.e. without the application of a magnetic field. There have not been many experimental studies of the interactions between magnetic domains and APBs and/or twin boundaries under the influence of an applied magnetic field. In order to tailor material properties associated with MFIS, a fundamental understanding of the behavior of magnetic domain walls and their interactions with microstructural features under the influence of an external magnetic field is needed. This was the primary motivation for the research presented in this paper.

The phenomenon of MFIS has been observed mostly in modulated martensitic structures. Magnetic domain configurations in five-layered (5M) and seven-layered martensites have been studied by several researchers using a variety of techniques, including Lorentz-mode transmission electron microscopy (LTEM), Types I and II magnetic contrast scanning electron microscope imaging, magnetic force microscopy and polarized light optical microscopy, to mention only a few [8–11]. Ge et al. have investigated the magnetic domain structure in 5M martensite in different orientational variants with a garnet indicator film in the magneto-optical imaging mode [9]. They reported that the domain structure inside a twin variant varies from a 180° domain pattern to a maze-like pattern, depending on the orientation of the easy axis inside the twin variant. The resolution of this technique, however, is not sufficient to reveal the transition of the magnetic domain structure across a twin boundary. We provide such details in the present study.

In a recent article, Lai et al. [10] studied the magnetic domain structure on different {100} faces of a 5M martensite crystal. They reported that the maze-like and 180° domain patterns are not just surface domain features, but penetrate deeper into the bulk volume of the material. Since the models developed to explain magnetic field-induced strain assume that the domain structure at the surface is valid throughout the volume of the material, such observations are encouraging for the development of theoretical models of the magnetic field-induced strain.

Chopra et al. observed magnetic field-induced twin boundary motion in an Ni₂MnGa MSMA with an interference-contrast-colloid technique [12]. The volume fraction of certain twins was observed to increase with an applied magnetic field, giving rise to macroscopic strain. The sam-

ple coercivity was attributed to pinning of domain walls at the twin boundaries. In a recent study, Armstrong et al. reported that the magnetostatic coupling between domains belonging to adjacent twins can give rise to an energy barrier to the motion of domain walls under an applied magnetic field [13]. It should be noted that the martensitic microstructures in MSMAs can contain extremely fine twin variants (ranging from a few nm to a few µm). Furthermore, the APBs resulting from the B2′ to L2₁ atomic ordering transformation in the Ni–Mn–Ga system are only a few atomic layers thick. The magnetic domain structure associated with such fine microstructural features cannot be resolved with some of the lower resolution techniques, such as magneto-optical or Bitter methods.

The association of APBs with 180° magnetic domain walls has been observed in other Heusler alloys, such as Cu₂MnAl [14]. Venkateswaran et al. [15] investigated the interactions between magnetic domains and APBs in austenitic Ni-Mn-Ga alloys in considerable detail. They observed that conventional TEM two-beam imaging using the superlattice reflections could not reveal the presence of anti-phase boundaries. The invisibility of APBs was attributed to the large extinction distances for the {111}-type superlattice reflections. However, they reported that the APBs can be observed indirectly in Lorentz mode, owing to their unusual magnetic contrast. APBs that are not coincident with a 180° wall show a double fringe contrast in out-of-focus Fresnel images. It has been postulated that APBs resulting from a B2' to L2₁ transformation contain regions that are locally disordered, such that the average spacing of Mn atoms is shorter than that in the L2₁ structure [16]. The smaller spacing is believed to make the Mn-Mn exchange interaction antiferromagnetic in nature, as opposed to the surrounding matrix, which is ferromagnetic. Thus, APBs exist as thin antiferromagnetic layers in an otherwise ferromagnetic L2₁ matrix. One of the important conclusions from Venkateswaran et al.'s work was that the magnetic induction across an APB need not change its direction unless a 180° wall coincides with an APB [15]. In another study [8], Venkateswaran et al. reported that APBs play an important role in preserving the magnetic domain structure of austenite throughout both the martensitic and para-to-ferromagnetic transformations. They used in situ LTEM to observe the changes in magnetic domain structure in the austenitic Ni-Mn-Ga alloy by cooling the sample through two important transformation temperatures, M_s and T_c . The magnetic domain memory across both the ferroelastic and ferromagnetic transformation was attributed to the pinning of magnetic domain walls by anti-phase boundaries.

These studies confirm that APBs strongly influence the magnetic microstructure of MSMAs in the demagnetized state. It is, however, imperative to observe the magnetic domain wall motion in the presence of APBs under the application of a magnetic field. Yano et al. [17] investigated the motion of magnetic domain walls in an austenitic Ni₂Mn(Al,Ga) alloy by applying a magnetic field during

Lorentz-mode observations. The domain wall motion was found to be intermittent rather than continuous because of pinning at APBs. Since MFIS occurs in the martensitic state, it is essential to study the motion of domain walls in the presence not only of APBs but also of martensite twin boundaries, which are strong pinning sites. In the present study, we provide LTEM observations in a 5M modulated microstructure of an Ni–Mn–Ga alloy under the application of a magnetic field. The interactions of magnetic domain walls with APBs as well as martensite twin boundaries are reported.

2. Materials and experimental methods

A single crystal of Ni_{49.9}Mn_{28.3}Ga_{21.8} was obtained from AdaptaMat Ltd., Finland for the in situ magnetization studies presented in this paper. The values of the martensitic start temperature (M_s) and the Curie temperature (T_c) , as provided in the manufacturer's data sheet, were 43 °C and 99 °C, respectively; the maximum available MFIS was reported to be 5.5%. The crystal was received in the form of a thin rectangular strip of 140 µm thickness which was spark cut from a larger crystal; the strip edges were along the cube directions of the original austenitic unit cell. From this crystal, 2.5 mm \times 2.5 mm \times 140 μ m pieces were cut for jet electropolishing. The samples were directly electropolished without any mechanical polishing in an electrolyte containing 95% ethanol and 5% perchloric acid. The voltage and temperature of the bath were maintained at 11 V and −40 °C, respectively. Prior to electropolishing, the samples were heated to 70 °C (i.e. above the M_s temperature) and cooled to room temperature to achieve a thermally induced multi-variant martensitic state.

TEM observations confirmed that, at room temperature, the sample was indeed in a multi-variant martensitic state with a 5M modulated structure. The magnetic domain structure in the demagnetized state was studied in LTEM mode on an FEI Tecnai F20 microscope with a dedicated Lorentz pole piece. Phase reconstructions were carried out, starting from through-focus Fresnel images, using the transport-of-intensity equation approach, described in more detail in Refs. [18,19].

In situ observations were carried out in a field emission JEOL 2100F microscope at the Argonne National Laboratory. An in situ magnetizing sample holder designed by Hummingbird Scientific was used to study the field-induced motion of magnetic domain walls. The sample was positioned in a cavity between two copper coils which act as an electromagnet, creating a field in the plane of the foil (perpendicular to the incident electron beam). The direction of the field was along the primary axis of the sample holder. The electromagnet was powered by a Keithley 2400 SourceMeter controlled via a National Instruments USB GBIB adapter and a custom LabView application. The current was increased in steps of 2.5 mA, which corresponds to a magnetic field step size of 3–5 Oe. Since the applied magnetic field causes deflections in the trajectory

of the electron beam, the beam must be corrected with the deflector coils to acquire a series of images from a given area of the sample. Images were recorded only when a change in the configuration of domain walls was observed. The field was increased from 0 to about 300 Oe in the positive direction, beyond which the deflector coils could no longer correct the deflections caused by the applied magnetic field. The field was then reduced to zero and the current was reversed; in this direction, the field could be increased to about -500 Oe. Although the holder is capable of applying a higher magnetic field strength (up to $\approx 700 \, \text{Oe}$), the limited ability of the beam deflector coils to correct the field-induced beam deflections makes it impossible to observe LTEM images at the highest field strengths. Hence, in this paper we report on magnetic domain wall motion for a magnetic field range of [+300, -500] Oe.

3. Results and discussion

3.1. Interactions between magnetic domain walls and APBs

Fig. 1a–c shows a Fresnel image series from an area that contains a spear-shaped band of twin variants. The electron beam is oriented close to the $[0\,1\,0]_C$ zone axis orientation, where the subscript C refers to the fact that the indexing is performed with respect to the cubic reference frame of the parent austenite crystal. Magnetic domain walls appear as bright or dark lines, as indicated by black and white arrows in Fig. 1a and c. Note the reversal of contrast in the under- and over-focused images. The color map of the integrated magnetic induction in Fig. 1f shows that this pair of domain walls encloses a domain whose magnetization points towards the left (green color on the color wheel). Note that the integrated induction maps shown in this paper are equivalent to magnetization maps.

The curved dark features in the Fresnel images are bend contours (indicated by white arrows in Fig. 1b) arising from diffraction effects. Although these contours do not contain magnetic contrast, they can give rise to image artifacts in the reconstructed phase maps. Bend contour artifacts often can be attributed to difficulties in achieving perfect alignment of the individual Fresnel images. Several such artifacts are indicated by white arrows in Fig. 1b and f. The contrast reversal corresponding to the magnetic domain walls is sufficiently prominent to distinguish them from the bend contours. During application of a magnetic field, the magnetic domain walls move, providing a clear illustration of the changes in the magnetization configuration inside the sample.

The microstructure shown in Fig. 1 contains two different kinds of twin variants with a markedly different magnetic domain structure. The spear-shaped twin variants

¹ For interpretation of color in Figs. 1–3 and 5, the reader is referred to the web version of this article.

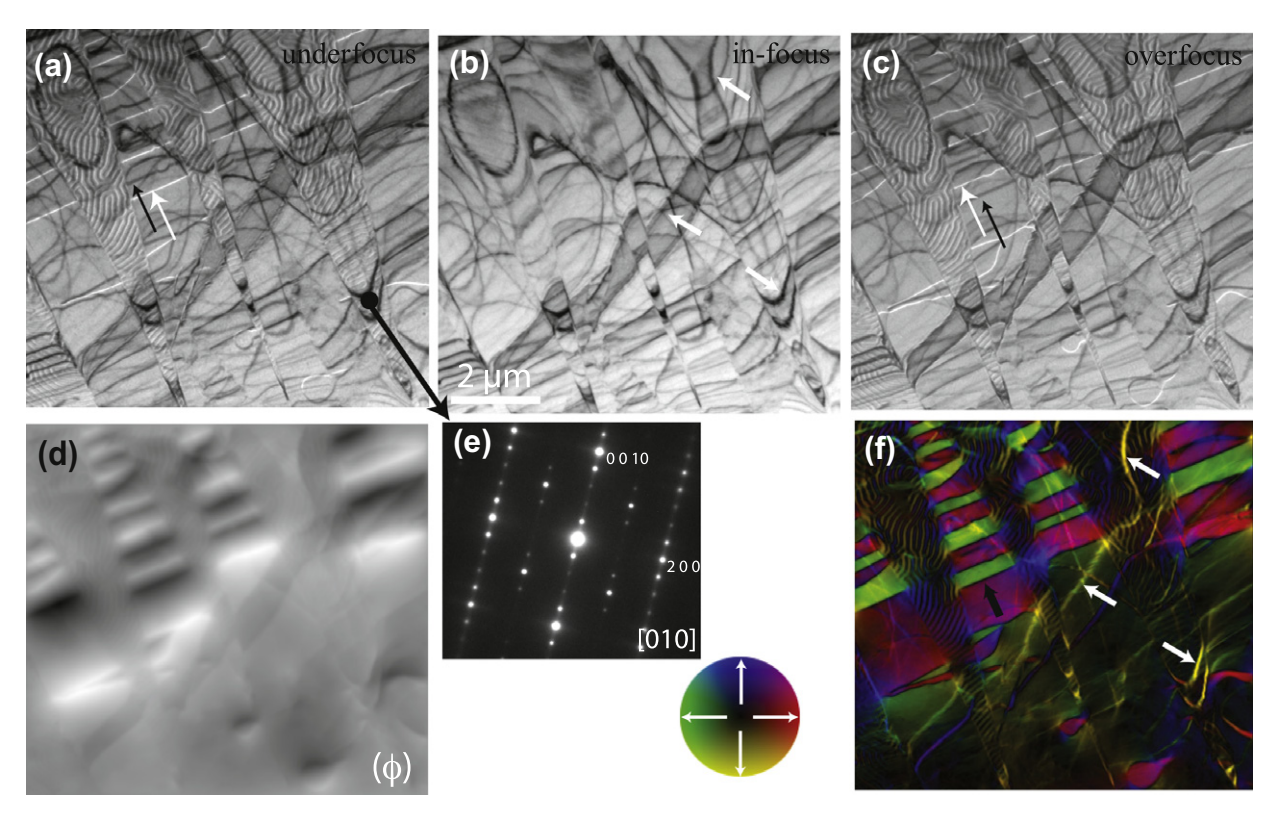


Fig. 1. Magnetic domain structure across a band of twin variants. (a–c) A Fresnel series of images. (d) A map of the reconstructed phase inside the sample. (e) A [010] zone axis diffraction pattern from a spear-shaped variant. (f) A color map of integrated magnetic induction inside the sample. The color wheel indicates the direction of magnetic induction corresponding to a particular color. Note that near bend contours, the color map may show incorrect colors as a consequence of numerical artifacts.

contain a maze-like magnetic domain structure, indicative of an out-of-plane magnetization direction. Diffraction analysis was performed in the conventional imaging mode to determine the orientation of the twin variants. Fig. 1e shows the $[010]_C$ room temperature diffraction pattern obtained from a spear-shaped twin variant with a 5M modulated structure. The $(101)_C$ planes are modulated along the $[10\overline{1}]_C$ direction. The shuffling of $(101)_C$ planes in the 5M structure takes place in such a way that every fifth $(101)_C$ plane is at its original position. In this notation, the magnetic easy axis is along the $[010]_C$ direction (b) direction), which is the cube axis that has undergone maximum contraction. Note that the magnetic easy axis is usually specified as the c axis. However, here we employ a different notation to be consistent with the monoclinic notation for the 5M modulated structure published in a recent article [20]. As the modulation direction in the spear-shaped variants lies in the plane of the foil, the magnetic easy axis is perpendicular to the plane of the foil, which explains the formation of the maze-like magnetic domain patterns inside these variants. On the other hand, the regions between the spear-shaped variants have an inplane magnetization direction. The integrated induction map in Fig. 1d reveals that the magnetization direction changes by 180° (from green to red) across these walls. Such 180° domain wall patterns are commonly observed in the demagnetized state of magnetic shape memory alloy

crystals when the preferred magnetization direction lies in the sample plane.

Fig. 2a-c shows the changes in the domain structure when a magnetic field is applied in the plane of the foil. Fig. 2d–f is the corresponding color maps of the integrated magnetic induction, obtained by phase reconstruction. The direction of the applied magnetic field, which is roughly at an angle of 30° to the horizontal direction, has been indicated on the color wheel. The easy axis directions E1 and E2 for adjacent twin variants have been labeled in Fig. 2d. In general, the movement of domain walls was observed to happen abruptly, rather than in a continuous fashion. As the field was increased in the positive direction, domain wall motion was initiated in the regions surrounding the spear-shaped variants. The black arrows in Fig. 2b indicate the direction of movement of the walls. There are fewer domain walls at locations 1 and 2 in Fig. 2b than in a. The 180° walls started to move under a field of 33 Oe in such a way that the area fraction of the green domains was reduced. This is apparent in Fig. 2e, which corresponds to an applied field of 85 Oe. These observations are consistent with the magneto-mechanical model proposed by Karaca et al. [21]. The saturation of an individual twin variant is accomplished by the motion of 180° domain walls that are already present in the demagnetized state. Another important observation in Fig. 2b and c is the bowing of the domain walls indicated by black arrows at locations 3 and

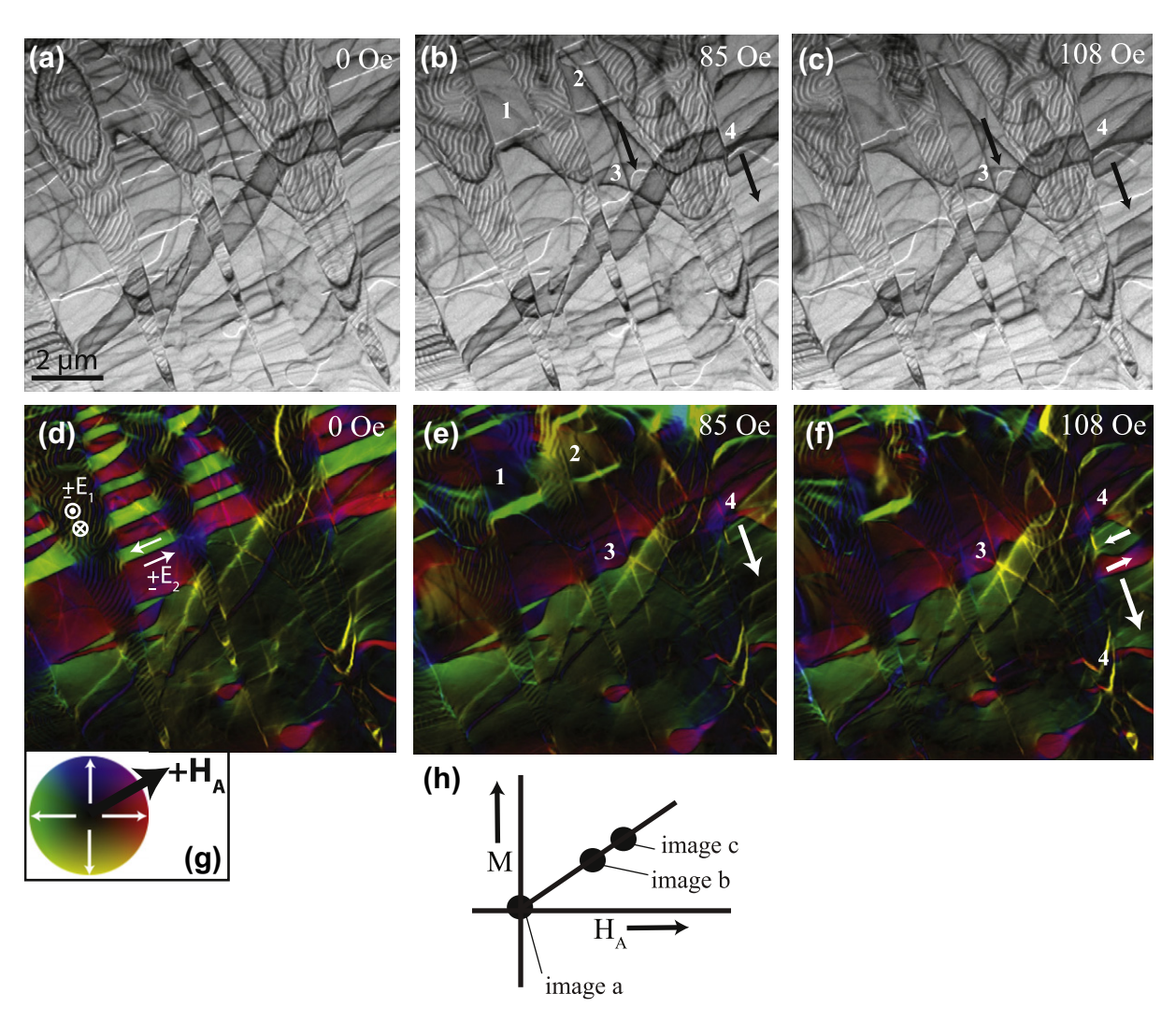


Fig. 2. Changes in the magnetic domain structure with increasing magnetic field. (a–c) Fresnel images recorded at different magnetic field values. (d–f) The corresponding color maps of the integrated magnetic induction. The direction of the applied magnetic field (H_A) is indicated on the color wheel. Note that the hysteresis curve is only schematic and illustrates where along the magnetization cycle the individual LTEM observations were carried out.

4. This bowing was attributed to the presence of anti-phase boundaries at these locations. Conventional two-beam TEM imaging using superlattice reflections could not reveal the presence of APBs in the martensite structure. However, a double fringe contrast, as reported by Venkateswaran et al. [15], was observed at these locations in the out-of-focus Fresnel images, indicative of the presence of APBs.

With a further increase of the applied field, the 180° domain wall pinned at location 4 in Fig. 2b was released. The phase map at a field of 108 Oe shows that the released wall leaves behind a domain that retains the magnetization direction prior to the passage of the wall (green color). Note that before the passage of the 180° wall, the magnetization across the APB was the same (green color). However, after the wall has passed, the APB separates domains with anti-parallel magnetization direction (green to red, indicated by a pair of white arrows in Fig. 2f); in other words, a segment of APB now coincides with a

180° wall. The green domain at location 4 in Fig. 2f is enclosed by two crystallographic features: an APB on the right and a twin boundary on the left. This serves as a nice example of how crystallographic features play a significant role during the magnetization cycle of this material.

Fig. 3a–d is Fresnel images illustrating the interaction between the magnetic domain wall and the APB at a higher magnification; Fig. 3e–g is color maps of the integrated magnetic induction corresponding to (a), (c) and (d) respectively. Fig. 3a shows a magnetic domain wall that coincides with the segment *op* of an APB. The direction of movement of the domain wall is indicated by the black arrow. As the domain wall is pinned by the APB at this location, increasingly higher fields were required to cause further motion of the wall. Lapworth and Jakubovics [14] stated that magnetic domain walls can be repelled by APBs. According to them, the APBs exist as curved surfaces, so that the creation of a 180° wall at an APB requires additional energy in the form of exchange and anisotropy energies. This may

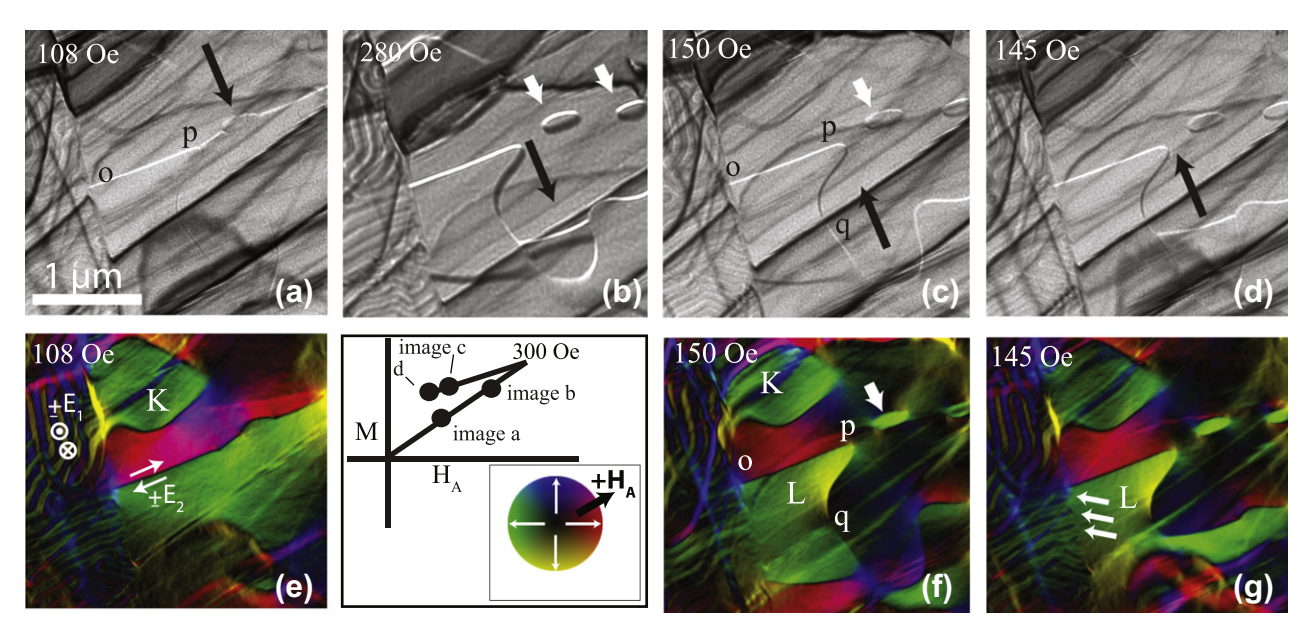


Fig. 3. The interaction of a 180° domain wall with an APB under increasing and decreasing magnetic field. (a–d) Fresnel images showing the location of domain walls at different values of magnetic field indicated at the top left corner. (e–g) Color maps of the integrated magnetic induction at different field values.

explain why increasingly higher fields were required to drive the domain wall forward against the APB. Fig. 3b shows the position of the domain wall at a field of 280 Oe; the wall has started to follow the curvature of the APB.

The field was then increased to 310 Oe, but limitations of the microscope defection coils did not allow for direct image observations. The field was then reduced back to 280 Oe, when it was observed that the domain wall had crossed the APB at some higher value of magnetic field. However, it did not return to the same position as shown in Fig. 3b at 280 Oe. Further reduction in the magnetic field was necessary to initiate the reverse motion of the wall through the APB. Fig. 3c shows the location of the wall at 150 Oe. A comparison between the color maps of Fig. 3e and f shows that the segment pq of the APB, which had identical magnetization on both sides of the boundary at 108 Oe, now separates regions with different magnetization directions at 150 Oe. In other words, the APB has pinned a segment of a 180° wall during the propagation of the original domain wall segment. The green domains, labeled K and L in Fig. 3f, are enclosed by an APB on the right and a twin boundary on the left. The connection between the green domain, L, and the maze structure is shown by a series of white arrows in Fig. 3g. It can be concluded that the APB segments that run across the twin boundary have retained the original state of magnetization inside the green domain during the motion of the domain wall. This series of Lorentz micrographs clearly demonstrates how APBs resist the process of magnetization.

As the field is reduced further to 145 Oe, the original domain wall begins to move in the opposite direction, shown by the black arrows in Fig. 3c and d. It should be

noted that the field was reduced by nearly 150 Oe (from 300 to 145 Oe) to initiate the reverse motion of this wall. This provides an estimate of the pinning strength of the APB. Another interesting feature in Fig. 3b and c is the presence of two bubble-like domains indicated by white arrows, which also retain their original magnetization direction (green). These were also identified as APB segments that completely enclose an ordered domain.

The magnetic domain structure upon reducing the applied field value to 0 Oe is shown in Fig. 4c, which looks markedly different from the initial demagnetized state shown in Fig. 4b. This is direct microstructural evidence for the existence of hysteresis in this material. Various crystallographic defects impede the reversible motion of domain walls; they can locally reduce the domain wall energy, thereby resisting its further movement. Fig. 4d shows the same area at the beginning of the second magnetization cycle. The magnetic domain structure is again different from either Fig. 4b or c.

The applied field was increased in the negative direction to follow further changes in the magnetic domain structure. Fig. 5a and b shows Fresnel images at +127 and -200 Oe, with the corresponding color maps in (c) and (d). Several green and red domains enclosed by APBs have been marked with black arrows in the Fresnel images and white arrows in the color maps. The magnetic domain wall motion showed similar characteristics as for the positive increments of the applied field in the sense that the domain walls were once again pinned by APBs. However, the APBs acting as pinning centers at -200 Oe were different from those at +127 Oe. Note that the field is now increased in a direction that favors the formation of "green" domains. Hence, the motion of domain walls was restricted by APBs

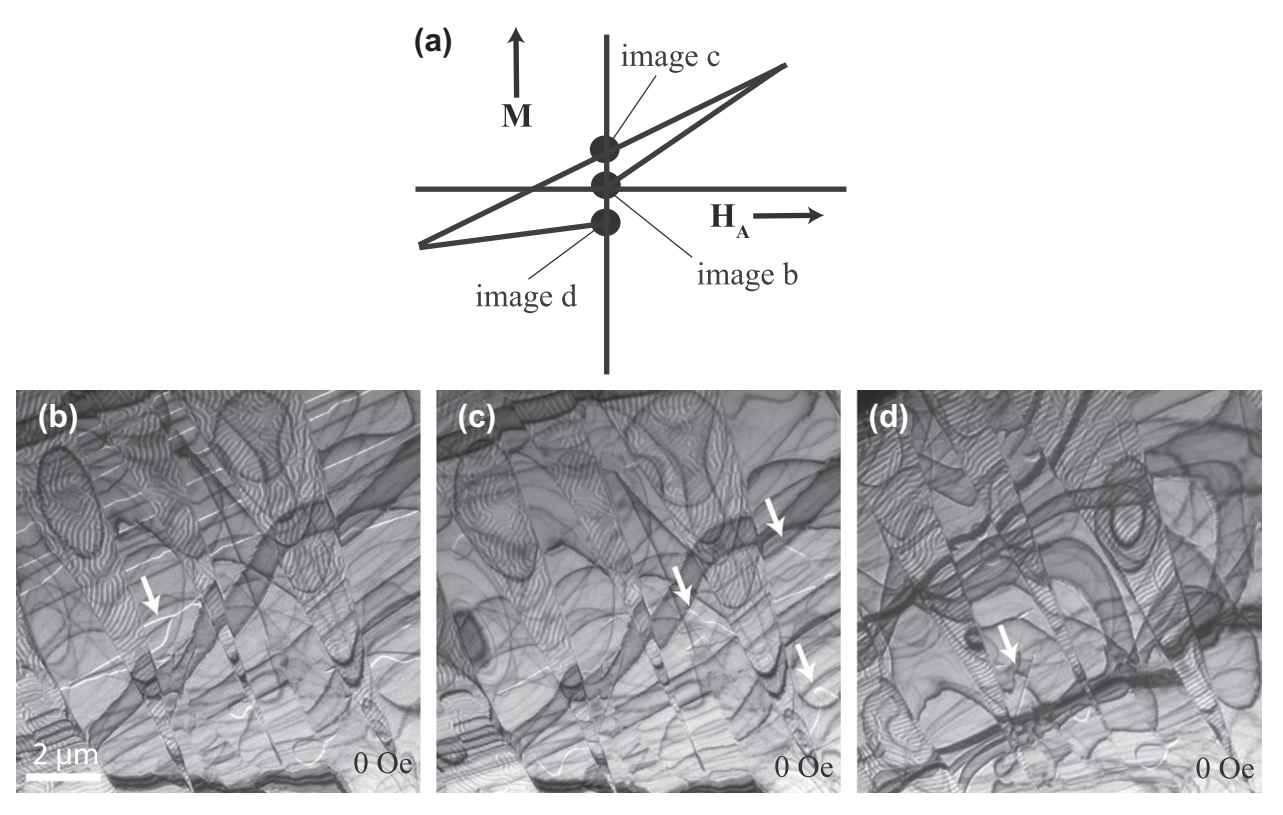


Fig. 4. Magnetic domain structure at 0 Oe for three different stages of the M vs. H curve.

which enclose domains with an opposite magnetization direction (red domains) to the applied field. It can be seen that the magnetic contrast associated with APBs at location 1 (see the Fresnel image at -200 Oe) has disappeared. Since those APBs were enclosing domains with magnetization parallel to the applied field, they do not act as pinning sites.

It is important to note that APBs that run across twin variant boundaries are very efficient pinning sites. This may be related to how the magnetostatic coupling between twin variants influences the domain wall motion. Armstrong et al. [13] observed domain wall motion in a twinned crystal of a Co-Ni-Ga alloy under the application of a magnetic field. They reported that the magnetostatic coupling across twin variants can act as an energy barrier, increasing the resistance to domain wall motion. Our observations confirm that such a coupling indeed exists and is mostly responsible for pinning of domain walls at the twin interface. As the magnetic easy axis changes abruptly across a twin boundary, magnetic free poles can be created, thereby increasing the stray field and the demagnetization energy. To avoid this situation, the twins remain coupled through magnetostatic interactions, thereby reducing the overall magnetostatic energy. The series of white arrows in Fig. 3g shows how the green domain enclosed by an APB (region L) is coupled to the maze-like structure in the adjacent twin variant. The APBs that run across the twin variants may provide easy pathways for the magnetostatic coupling across twin variants. Hence, the combined pinning effect of a twin boundary and an APB leads to the marked sites in Fig. 5 being strong pinning centers.

The observations of the movement of 180° domain walls inside individual twin variants must be seen in the light of earlier studies on Ni-Mn-Ga alloys with a similar composition. Lai et al. [22] used a magneto-optical imaging technique to study the change in magnetic domain structure associated with martensite twin variants in an Ni-Mn-Ga alloy. They observed that when a magnetic field was applied to variants whose easy axes were perpendicular to the field, new variants were nucleated with easy axis parallel to the field. Such variants grew at the expense of adjacent variants by twin boundary motion. The magnetization process of a material usually involves the motion of domain walls corresponding to the change in configuration of magnetic domains. Interestingly, Lai et al. did not observe movement of 180° domain walls located inside an individual twin variant during the magnetization cycle. This observation is in stark contrast with our observations and with a magneto-mechanical model proposed by Karaca et al. to explain the MFIS [21]. Karaca et al. postulated that magnetic domain wall motion and magnetization rotation inside an unfavorably oriented variant should occur at field strengths that are much lower than those required to induce twin boundary motion. However, Lai et al. did not observe the motion of 180° walls, even at the critical field necessary to induce twin boundary motion. In our case, magnetic fields as low as 33 Oe were sufficient to acti-

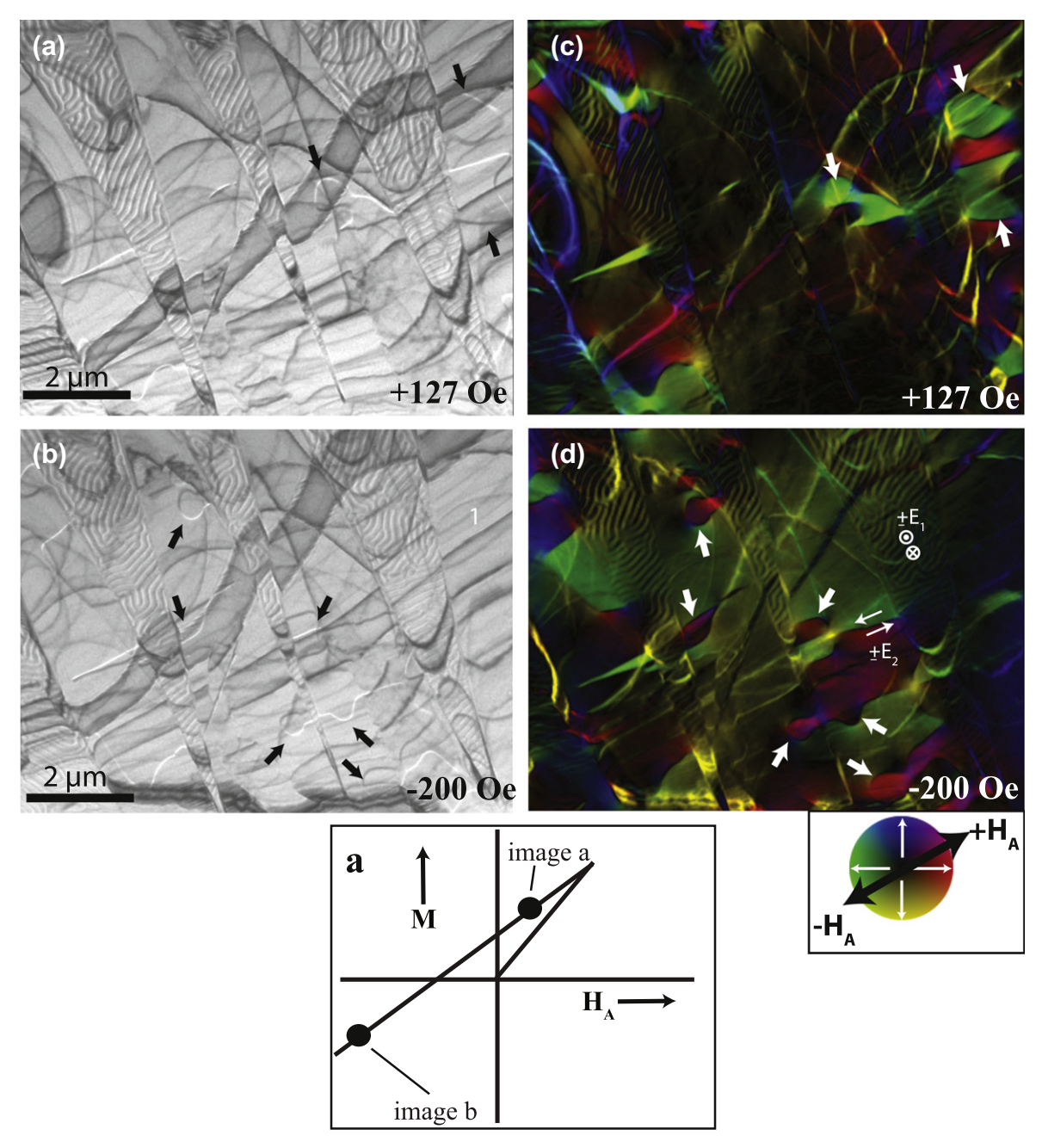


Fig. 5. Pinning of magnetic domain walls under positive and negative magnetic fields. (a and b) Fresnel images at +127 and -200 Oe. (c and d) The corresponding color maps of integrated magnetic induction.

vate the motion of 180° magnetic domain walls inside a twin variant. A possible reason for such a contradiction in the observations may be the difference in specimen thickness (4.5 mm in case of Lai's study vs. ≈100 nm in our study). It is worthwhile noting that Armstrong et al. [13] also observed the movement of 180° walls within the twin variants of a Co−Ni−Ga crystal with a thickness of 0.89 mm. Theoretical models concerning the movement of domain walls in soft magnetic alloys point out that eddy current effects can dampen the domain wall motion in the case of thicker samples [23]; this may explain the discrepancies between these observations.

3.2. Maze-like domain structure under the influence of an applied field

The maze-like domain structure inside the spear-shaped variants was more stable with respect to the applied field than the 180° wall pattern in the adjacent twin variants. No significant changes in the maze-like domain structure were observed for applied fields up to about 100 Oe in both positive and negative directions. At some locations, however, movement of domain walls in a neighboring twin variant caused appreciable changes in the maze-like domain structure. Fig. 6a shows the maze-like domain structure

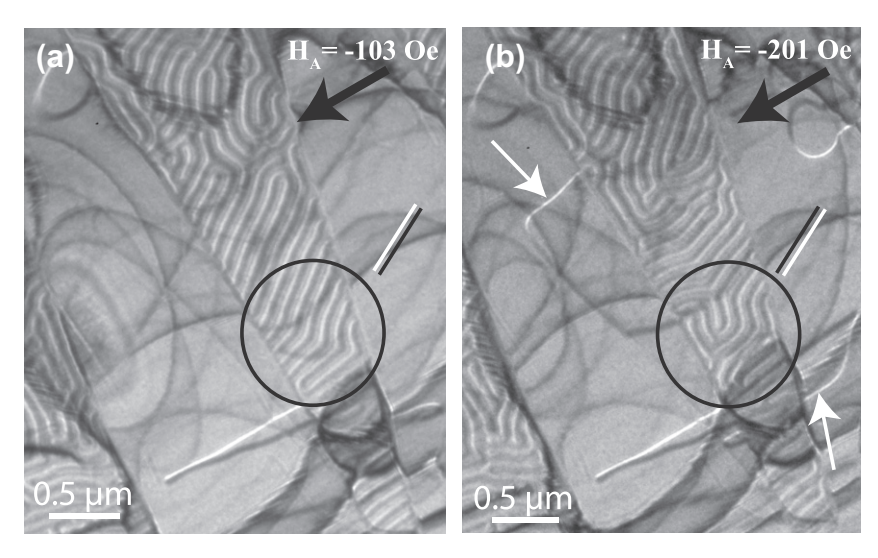


Fig. 6. Local changes in the maze-like domain structure with changes in the domain structure of the adjacent twin variant.

at a field of -103 Oe. As the field was further increased to about -201 Oe, the magnetic domain wall structure in the adjacent twin was observed to change at locations indicated by white arrows in Fig. 6b. Projected induction color maps revealed that these domain walls were pinned on APBs. As a result, the maze structure in the spear-shaped twin changes to a different configuration (see the encircled region). There is also a pairwise reversal of the contrast associated with the magnetic domain walls in the maze structure; a pair of black and white lines have been overlaid on the images to clarify this reversal. Since the changes in adjacent twin variants were related to domain walls pinned on APBs, it can be speculated that the APBs crossing the twin boundary must be playing a role in this process. Such local changes in the maze-like domain structure were attributed to the magnetostatic coupling between the twin variants discussed in the earlier section. However, the exact mechanism behind these changes is unclear at this time.

At larger values of the applied magnetic field, the mazelike domain structure starts reorienting itself into a configuration with parallel domain walls. Fig. 7 shows the domain structure inside the spear-shaped variants at a field of -480 Oe. The domain walls have become straight (see the encircled region) and now run parallel to the applied field direction indicated by the black arrow in the bottom left corner. The straightening effect was more prominent in the narrower region of the twins. Fresnel images are usually recorded with an objective aperture to remove the stray contrast arising from diffraction effects. However, at -480 Oe, the beam was deflected so strongly that the region of interest could not be viewed with the objective aperture inserted; the image was therefore recorded without an objective aperture. As a result, some diffraction contrast is visible in this out-of-focus image as diffuse white features (white arrows in Fig. 7). The straightening effect is likely driven by the Zeeman energy associated with the domain walls in an applied field; the magnetization rota-

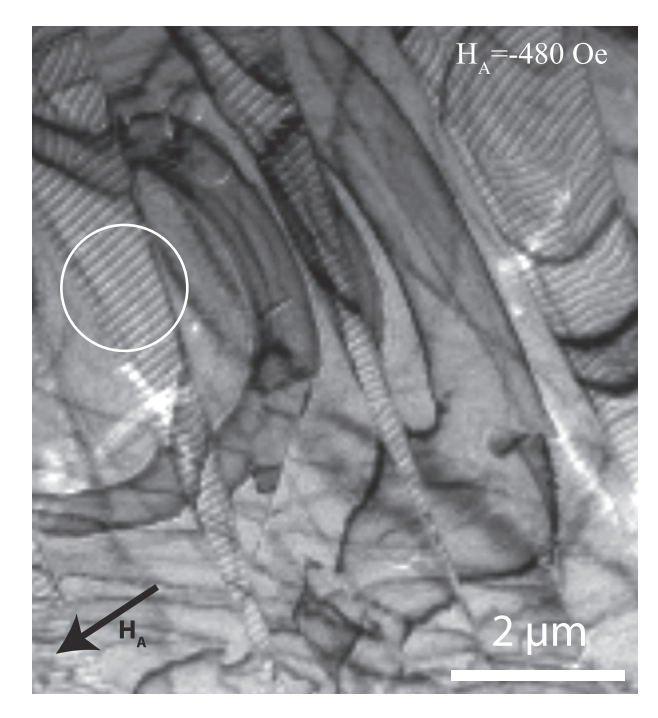


Fig. 7. Alignment of magnetic domain walls along the field direction in the maze-like domain structure. This image was captured from a low resolution movie, which caused pixelation artifacts in the domain walls.

tion across the domain wall has a lower Zeeman energy when the rotation plane is normal to the applied field, which leads to straightening of the walls. Note that this rotation occurs at much lower fields than the final magnetization rotation that would lead to saturation.

3.3. Pinning of magnetic domain walls at twin boundaries

Fig. 8a–f shows the change in magnetic domain structure associated with a band of twin variants with easy axis in the plane of the foil. Magnetic domain walls are visible as alter-

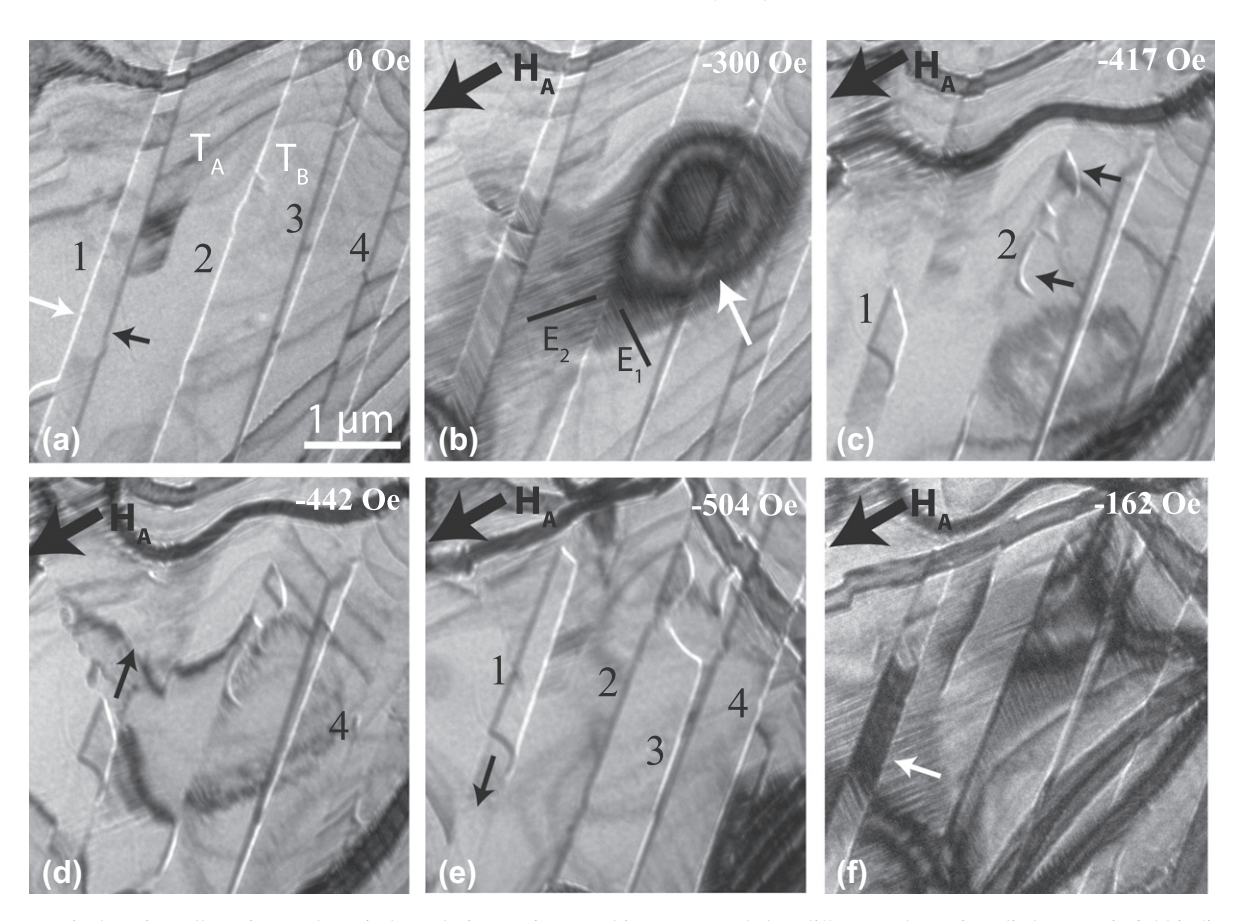


Fig. 8. Magnetic domain wall motion at the twin boundaries. (a–f) Fresnel images recorded at different values of applied magnetic field indicated at the top right corner. Note that the striations visible inside the twins are due to stacking faults.

nating black and white lines, strongly pinned at, and parallel to, the twin boundaries. A pair of domain walls is indicated by white and black arrows in Fig. 8a, as well as several pinned walls at locations 1-4. Upon increasing the field from 0 to ± 300 Oe, these domain walls remained pinned at the twin boundaries. Observations above an applied field value of 300 Oe could not be made because of the limitations of the beam deflector coils. In the reverse direction, the domain walls again remained strongly pinned at the twin boundaries up to -300 Oe. Fig. 8b shows the region of interest at an applied field of -300 Oe; the walls are still pinned at the twin boundaries. However, note that the background diffraction contrast (dark regions associated with bend contours, as indicated by a white arrow) in Fig. 8b has changed, possibly because of a slight bending of the foil due to the applied field or because of magnetostrictive strains. The striations indicated by black lines in Fig. 8b are due to stacking faults in the individual twin variants; the direction of these striations, which is parallel to the local easy axis direction, changes by almost 90° across each twin boundary.

As the field value was further increased to about -400 Oe, the domain walls at locations 1 and 2 became unpinned from the twin boundaries. The process of unpinning occurred abruptly and the original domain walls

broke into smaller segments. Some of these segments are indicated by black arrows at location 2 in Fig. 8c, which was acquired at -417 Oe. These segments nucleated at the twin boundaries and showed a reverse contrast as compared to the original domain wall. This contrast reversal is clearly observed at location 1 in Fig. 8c, where the nucleated domain walls enclose a region of the twin variant with possibly a different magnetization direction than the surrounding region. With a further increment in the magnetic field, the domain walls at location 4 were unpinned, as shown in Fig. 8d, which was recorded at -442 Oe. As the field was increased, the newly formed domains grew in size along the twin boundaries. The direction of domain growth is indicated by a black arrow in Fig. 8d. The growth of a domain is clearly visible at locations 1 and 2 in Fig. 8e, acquired at -504 Oe. It can also be seen that the domain wall at location 4 has reappeared with a reverse contrast as compared to Fig. 8a. No observations could be made beyond a field value of -504 Oe, due to the difficulties mentioned before. Hence, the field was reduced towards 0 Oe. Below -400 Oe, the original domain wall structuredid not return; instead, the newly formed domain states grew in size and a magnetic domain structure with exactly reversed contrast compared to the original structure was found to be stable down to 0 Oe. The white arrow near

the location 1 in Fig. 8f, recorded at -162 Oe, shows that the domain wall has grown along the length of the twin boundary. Although the diffraction contrast is obscuring some of the magnetic contrast in this image, it is clear that the domain walls in Fig. 8f have an exactly reversed contrast as compared to Fig. 8a.

It is well known that the MFIS involves the movement of multiple ferroic boundaries: ferroelastic boundaries (twin boundaries) and ferromagnetic boundaries (magnetic domain walls). As the magnetic domain walls coincide with martensite twin boundaries, both magnetic domain walls and twin boundaries should move under the application of magnetic field. However, at this time, it is not clear if the magnetic domain walls and twin boundaries move simultaneously or independently. Paul et al. [24] have tackled this problem by using micro-magnetic equations for the case of two crystallographic twin variants with different orientations of their magnetic easy axis. They calculated the equilibrium positions of the twin boundary and the magnetic domain wall under the application of a magnetic field by considering micro-magnetic expressions for the exchange, anisotropy, strain and Zeeman energies. They concluded that, if the magnetic driving force is less than the strain energy barrier, the magnetic domain wall motion always leads the twin boundary motion. In our observations, the maximum applied magnetic field (\approx 500 Oe) was much less than that required for twin boundary motion (3–4 kOe). A magnetic domain wall coincident with the twin boundary became dislodged at a field of -400 Oe, so that the unpinning of a magnetic domain wall was observed at field values much lower than the critical magnetic field necessary to induce the twin boundary motion. Our observations are consistent with the theoretical predictions made by Paul et al. in the sense that magnetic domain walls are dislodged from twin boundaries before the occurrence of actual twin boundary motion.

4. Conclusions

The magnetic domain structure of a 5M modulated martensite in a $Ni_{49.9}Mn_{28.3}Ga_{21.8}$ alloy was investigated using in situ LTEM observations. The applied magnetic field, which was the driving force for the magnetic domain wall motion, was cycled from 0 to +300 Oe to -500 Oe and then back to 0 Oe. Significant magnetic domain wall motion was observed inside the twin variants. The most important observation results can be summarized as follows:

- (1) The magnetization process for an individual twin variant with magnetic easy axis in the plane of the foil involves motion of 180° domain walls. An applied field as low as 33 Oe was sufficient to activate the movement of 180° domain walls, consistent with the magneto-mechanical model proposed by Karaca et al. [21].
- (2) The 180° domain walls were often pinned at APBs. APBs were observed to enclose domains with magnetization direction opposite to the applied magnetic

- field, even at fields as high as 300 Oe; this observation is consistent with a higher coercivity of samples with a higher APB density, a known effect in the Ni–Mn–Ga system as well as in Cu–Mn–Al Heusler alloys [15,25]. APBs crossing the twin boundaries were very efficient pinning sites, since they might provide easy pathways for magnetostatic coupling between twin variants, thereby increasing the resistance to domain wall motion.
- (3) Twin variants with out-of-plane easy axis displayed a maze-like domain structure which was found to be much more stable with respect to the applied field than the 180° domain structure inside adjacent twins. No significant changes in the maze domains were observed up to a field of ± 100 Oe. At approximately 460 Oe, the magnetic domain walls inside the maze domains started to align parallel to the applied field direction. The straightening of domain walls is possibly related to the lowering of the Zeeman energy of the walls under the applied field.
- (3) The twin boundaries were also found to be strong pinning sites for domain walls. The walls that coincided with the twin boundaries became unpinned around -400 Oe. This result is consistent with theoretical predictions from micro-magnetic computations about the relative motion of domain walls and twin boundaries [24]. No twin boundary motion was detected in the applied magnetic field range of [-500,+300] Oe.
- (4) The magnetic domain structure for a particular field value was considerably different for the forward and reverse components of the hysteresis curve, providing direct experimental evidence for hysteretic behavior. Lattice defects, such as APBs and twin boundaries, locally lower the domain wall energy, hence larger fields are required to move the walls away from these features.

Acknowledgements

The results presented in this paper represent a portion of the Doctoral Thesis research of A.B. The authors would like to acknowledge Dr. Kari Ullakko for providing the Ni–Mn–Ga alloy. M.D.G. and A.B. would like to acknowledge the financial support from National Science Foundation, NSF DMR # 1005330. A part of this work was carried out at Argonne National Laboratory, a US Department of Energy, Office of Science Laboratory operated under contract DE-AC02-06CH11357 by University of Chicago Argonne, LLC. The funding for the JEOL Lorentz TEM was provided by US DOE, Division of Materials Science and Engineering, Office of Basic Energy Sciences. C.P. and A.K.P.L. would like to acknowledge the financial support from the DOE.

References

- [1] Sozinov A, Likhachev A, Lanska N, Ullakko K. Appl Phys Lett 2002;80:1746–8.
- [2] Wechsler M, Liebermann D, Read T. Trans AIME 1953;197:1503-15.
- [3] Bhattacharya K. Arch Rat Mech Anal 1992;120:201-44.
- [4] James R, Wuttig M. Philos Mag A 1998;77:1273-99.
- [5] O'Handley R, Allen S. In: Encyclopedia of smart materials. New York: Wiley; 2002. p. 936–51.
- [6] Likhachev A, Ullakko K. Euro Phys J B 2000;14:263-7.
- [7] Webster P, Ziebeck K, Town S, Peak M. Philos Mag B 1984;49: 295-310.
- [8] Venkateswaran S, Nuhfer N, DeGraef M. Acta Mater 2007;55: 5419–27.
- [9] Ge Y, Heczko O, Soderberg O, Hannula S. Mater Sci Eng A 2008;481–482:302–5.
- [10] Lai Y, Schafer R, Schultz L, McCord J. Appl Phys Lett 2010;96: 022507.
- [11] Mullner P, Clark Z, Kenoyer L, Knowlton W. Mater Sci Eng A 2008;481–482:66–72.
- [12] Chopra H, Ji C, Kokorin V. Phys Rev B 2000;61:R14913.
- [13] Armstrong J, Sullivan M, Romancer M, Chernenko V, Chopra H. J Appl Phys 2008;103:023905.

- [14] Lapworth A, Jakubovics J. Philos Mag 1974;29:253-73.
- [15] Venkateswaran S, Nuhfer N, DeGrae M. Acta Mater 2007;55:2621–36.
- [16] Young A, Jakubovics J. J Phys F: Metal Phys 1975;5:1866-83.
- [17] Yano T, Murakami Y, Kainuma R, Shindo D. Mater Trans JIM 2007;48:2636-41.
- [18] Paganin D, Nugent K. Phys Rev Lett 1998;80:2586-9.
- [19] De Graef M. Lorentz microscopy: theoretical basis and image simulations. In: De Graef M, Zhu Y, editors. Magnetic microscopy and its applications to magnetic materials of experimental methods in the physical sciences, vol. 36. Academic Press; 2000. p. 27–67.
- [20] Righi L, Albertini F, Pareti L, Paoluzi A, Calestani G. Acta Mater 2007;55:5237–45.
- [21] Karaca H, Karaman I, Basaran B, Chumlyakov Y, Maier H. Acta Mater 2006;54:233–45.
- [22] Lai Y, Scheerbaum N, Hinz D, Gutfleisch O, Schafer R, Schultz L, et al. Appl Phys Lett 2007;90:192504.
- [23] Bishop JJ. Magn Magn Mater 1984;41:261-71.
- [24] Paul D, Marquiss J, Quattrochi D. J Appl Phys 2003;93:4561-5.
- [25] Bouchard N, Swann P. In: Proceedings of the 7th international congress on electron microscopy. Soc. Française de Microscopic Electronique, Paris, France; 1970. p. 475–6.